VI International Conference on Particle-based Methods – Fundamentals and Applications
PARTICLES 2019
E. Oñate, M. Bischoff, D.R.J. Owen P. Wriggers, & T. Zohdi (Eds)

SOLID PARTICLE INTERACTION DYNAMICS AT CRITICAL STOKES NUMBER IN ISOTROPIC TURBULENCE

K. RAI*, M. FAIRWEATHER AND L.F. MORTIMER

School of Chemical and Process Engineering, University of Leeds, Leeds LS2 9JT, UK
*pmkr@leeds.ac.uk

Key words: Direct numerical simulation, Immersed boundary method, Isotropic turbulence, DLVO interaction, Agglomeration.

Abstract. Binary solid spherical particle-particle interactions are studied in forced isotropic turbulence at Re_λ = 29 and 197 using direct numerical simulation and an immersed boundary method. Isotropic turbulence in a periodic box is forced using a linear forcing method to maintain statistically stationary turbulence, with inter-particle interaction modelled using DLVO interaction forces which include attraction and repulsion due to van der Waals and electric double layer potential forces, respectively. Particle collisions are modelled using the inelastic hard sphere model with a coefficient of restitution of 0.4. The DLVO parameters are chosen to be representative of calcite particles, a simulant of nuclear waste material found in storage ponds in the UK. The Reynolds numbers chosen for the boxes are equivalent to typical values of Re_λ that are found in the bulk flow and viscous sub-layer regions of a turbulent channel flow at $Re_\tau = 180$. The techniques described are used to study the dynamics of critical Stokes number particles in turbulence by analysing probability density functions (PDFs) of collision statistics such as particle displacement and the particles' relative velocities to determine the likelihood of agglomeration. The results indicate that agglomeration can occur in both the Re_λ turbulent boxes considered. However, the occurrence is much more likely at lower Re_λ values due to the higher dispersion of kinetic energy after impact.

1 INTRODUCTION

Particle-laden turbulent flows occur commonly in both natural and industrial environments. Understanding of the dynamics of such flows is of interest to many industries. One application of relevance to the present work is in the nuclear industry. In the UK, most spent nuclear fuel and nuclear waste is stored in ponds or silos, often occurring as a solid-liquid slurry. Over many years the structural integrity of the ponds has been deteriorating and there is an increased need to transport the waste to other safe storage facilities. A key problem remains in knowing how best to transport the solid-liquid slurry in the most efficient, effective and safe way. The present work addresses this issue with the help of particle-laden flow and particle-particle interactions simulations.

One method of simulating particle-laden flows is to consider particles to be point-like, meaning that the particle diameter must be less than the smallest scales found in a turbulent flow, namely the Kolmogorov length scale. By using Lagrangian particle tracking (LPT) in

multi-phase fluids, i.e. through solving the equation of motion for each particle in the flow [1], a relatively good understanding of particle dynamics in fluid flows can be obtained. However, this method is inherently problematic since particles in nature are not point-like. For example, LPT does not accurately resolve all the forces acting on a particle. To overcome this limitation in LPT simulations a more fundamental approach is to use, for example, the immersed boundary method (IBM). IBM emerged from Peskin's work [2] in 1972 on the mathematical modelling of the heart. This method allows a particle to have a finite size and shape, which in turn allows the realistic capturing of all the forces acting on particles in all directions from the fluid. Over the years, authors such as Mark and van Wachem [3], and Tseng and Ferziger [4], have worked on the development of this method, with various degrees of accuracy. However, to date there has been no previous work implementing IBM with resolved DLVO forces, which are the forces that describe the interaction between electrically charged particles.

The novelty of the present work therefore lies in the implementation of IBM using DLVO forces to study the dynamics of interacting particles. Particles not only interact with the fluid turbulence but also with each other through DLVO forces. The study focuses on using IBM to elucidate particle dynamics and the likelihood of particle agglomeration in isotropic turbulent boxes at two Reynolds numbers, based on the Taylor microscale, of $Re_\lambda = 29$ and $Re_\lambda = 197$. Conclusions are drawn by analysing PDFs of the relative velocity and displacement of interacting binary particles for critical Stokes number, $St_k = 1$, particles obtained through ensembles of interactions. Such particles are considered since one question of interest in particle-laden flows is at what Stokes number (for a given concentration) do particles start to affect the flow and turbulence dynamics. Elghobashi [5, 6] has demonstrated that at solid volume fractions between 10^{-6} and 10^{-3} there exists a critical Stokes number. Below this value, particles are considered small and their response time is much smaller than the Kolmogorov time scale, with such low inertia particles prone to becoming trapped in vortical structures of the flow, increasing the fluid turbulence kinetic energy and its dissipation rate. Above the critical Stokes number, particles are considered large and are less likely to respond to local fluctuations in the fluid velocity field and, unlike small particles, are ejected from vortical structures. The net result is that these large particles attenuate the turbulence kinetic energy and its dissipation rate within the fluid flow.

2 METHODOLOGY

2.1 Fluid flow simulation

The spectral-element method code, Nek5000 [7], was used to perform direct numerical simulations of single-phase homogeneous, isotropic turbulent boxes at $Re_\lambda = 29$ and $Re_\lambda = 197$. The domain of the isotropic box was $2\pi \times 2\pi \times 2\pi$ which was resolved using $48 \times 48 \times 48$ elements of 7th order, such that there were $336 \times 336 \times 336$ (or a total of ~38M) nodes in each box. These elements were distributed uniformly inside each box. The Re_λ of the isotropic boxes was chosen to match the Reynolds number that is typical of the bulk flow ($Re_\lambda = 29$) and viscous sub-layer ($Re_\lambda = 197$) regions of a turbulent channel flow at shear Reynolds number, $Re_\tau = 180$.

The code solves the following governing fluid flows equations, i.e. the mass conservation

and Navier-Stokes equation:

$$\frac{\partial \boldsymbol{u}}{\partial t} + \boldsymbol{u} \cdot \nabla \boldsymbol{u} = -\nabla p + \frac{1}{Re} \nabla \cdot \boldsymbol{\tau} + \boldsymbol{f} \tag{1}$$

$$\nabla \cdot \boldsymbol{u} = 0 \tag{2}$$

where $\boldsymbol{u}$ is the fluid velocity field, p is pressure, Re is Reynolds number, τ is the viscous deviatoric stress tensor and $\boldsymbol{f}$ is an arbitrary forcing or source term.

Isotropic turbulence in each box was obtained by implementation of the linear forcing method proposed by Lundgren [8], and Rosales and Meneveau [9], who demonstrated that linear forcing proportional to the velocity in physical space gives the same result as forcing in spectral space, and that linearly forced boxes converge to a statistically stationary state that depends only on domain size and Reynolds number.

It was demonstrated by Rosales and Meneveau [9] that $\boldsymbol{f} = A\boldsymbol{u}'$, where $A = \epsilon/3u_{rms}^2$, ϵ is the dissipation rate and u_{rms} is the root-mean-square (rms) of velocity fluctuations in any direction since isotropy is ensured. This term is a force (in physical space) with an appropriate parameter A necessary to obtain statistically stationary isotropic turbulence. Energy is injected at a variable rate of A until steady state has been achieved. After that, energy is injected at a constant rate of A since both ϵ and u_{rms} will have reached their stationary values. The initial conditions used to initiate the simulations were:

$$\begin{aligned} u &= \cos(y) + \sin(z) \\ v &= \sin(y) + \cos(z) \\ w &= \cos(x) + \sin(y) \end{aligned} \tag{3}$$

The parameters used to obtain the isotropic boxes are presented below in Table 1.

Table 1: Values of the parameter A in $\boldsymbol{f} = A\boldsymbol{u}'$ used to obtain stationary isotropic turbulence.

Re_λ	29	197
A	0.0667	0.1667

2.2 Immersed boundary method

The immersed boundary method represented each particle using an icosphere with 320 triangular faces, as illustrated in Fig. 1. The centroid of each triangular face on the icosphere has associated with it a position and a velocity. The Dirichlet boundary condition at the surface of the icosphere was enforced such that $\boldsymbol{u}_F = \boldsymbol{u}_p + \boldsymbol{\omega}_p \times \boldsymbol{r}_f$ on each particle face, where $\boldsymbol{u}_p$ is the particle linear velocity, $\boldsymbol{\omega}_p$ is the particle angular velocity and $\boldsymbol{r}_f$ is the position vector from the centre of the particle to the centroid of a face.

To ensure the immersed boundary condition was met, a second-order accurate ghost-cell method was employed [4]. Every time-step, each cell in the domain was identified as external fluid, an internal ghost-cell or internal fictitious fluid. The ghost cell was defined such that the immersed boundary intersected the cell and contained the cell midpoint. Internal and external fluid cells are those either inside or outside of the immersed boundary, respectively. The

velocities at the ghost-cells were maintained each time-step such that, through trilinear interpolation across the three closest neighbouring cells, the fluid velocity on the boundary was exactly the local face velocity [10].

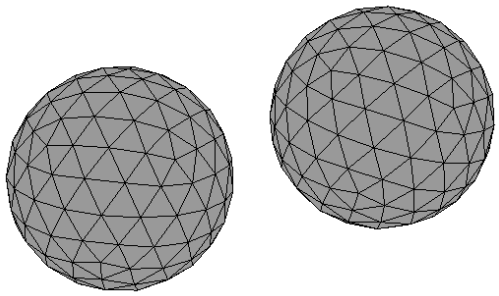

Figure 1: Icosphere mesh with 320 triangular faces.

The advection and rotation of each particle was derived from the hydrodynamic forces acting on an icosphere, as defined in Eq. (4) [10]:

$$F_j = \sum_{f=1}^{N_f} \left(-P^f \delta_{ij} + \tau_{ij}^f\right) n_j^f \, dS^f, \tag{4}$$

where the F_j is the total force acting on a particle, j is the current face, N_f is the total number of faces in a particle, P^f is the pressure interpolated at the centroid of the face, τ_{ij} is the viscous stress tensor, n_j^f is the unit normal vector to the face f and dS^f is the surface area of face f.

The orientation of a particle was tracked using quaternions. A unit quaternion describes the rotation of $\boldsymbol{v}$ by angle θ about the axis in the direction of $\boldsymbol{u}$ by $\boldsymbol{v'} = q\boldsymbol{v}q^{-1}$, where $q(v_0, \boldsymbol{q}) = cos(\theta/2) + sin(\theta/2)\boldsymbol{u}$, and $\boldsymbol{u} = u_1 i + u_2 j + u_3 k$ is a unit vector, θ is the angle of rotation and $\boldsymbol{v'} = q\boldsymbol{v}q^{-1} = \boldsymbol{v} + \boldsymbol{2}q_0(\boldsymbol{v} \times \boldsymbol{q}) + 2(\boldsymbol{v} \times (\boldsymbol{v} \times \boldsymbol{q}))$. The time evolution of the quaternion $\boldsymbol{Q}$ is described by the differential equation:

$$\frac{d\boldsymbol{Q}}{dt} = \begin{pmatrix} \frac{dq_0}{dt} \\ \frac{dq_1}{dt} \\ \frac{dq_2}{dt} \\ \frac{dq_3}{dt} \end{pmatrix} = \begin{pmatrix} q_0 & -q_1 & -q_2 & -q_3 \\ q_1 & q_0 & -q_3 & q_2 \\ q_2 & q_3 & q_0 & q_1 \\ q_3 & -q_2 & q_1 & q_0 \end{pmatrix} \begin{pmatrix} 0 \\ \omega_{x'} \\ \omega_{y'} \\ \omega_{z'} \end{pmatrix}, \tag{5}$$

where $\boldsymbol{\omega} = (\omega_{x'}, \omega_{y'}, \omega_{z'})$ is the angular velocity vector in the particle co-moving frame. The unit quaternions were normalised to one after each time step to minimise the error due to

floating-point precision issues. The corresponding governing equation for angular acceleration can be expressed as:

$$\boldsymbol{I}\,\frac{d\boldsymbol{\omega}}{dt} = \boldsymbol{T} = \sum_{i} \boldsymbol{r_i} \times \boldsymbol{F_i} \tag{6}$$

where $\boldsymbol{\omega}$ is the angular velocity of the sphere, $\boldsymbol{T}$ is the torque, $\boldsymbol{r_i}$ is the distance vector to the centroid of the face from the centre of a particle, $\boldsymbol{F_i}$ is the hydrodynamic force and $\boldsymbol{I}$ is the moment of inertia tensor of a solid sphere, given as:

$$\boldsymbol{I} = \begin{pmatrix} 2/5mr^2 & 0 & 0 \\ 0 & 2/5mr^2 & 0 \\ 0 & 0 & 2/5mr^2 \end{pmatrix}, \tag{7}$$

where m is the mass of the sphere and r is its radius.

Once the particle was advected, all pairs of particles were checked for potential collisions. The condition required for collision is the inter-surfacial distance is less than zero. The particles collided inelastically using a hard-sphere approach with the coefficient of restitution of 0.4 during the time of collision.

Particle-particle interaction was modelled using DLVO theory developed by Derjaguin and Landau [11], and Verwey and Overbeek [12]. It was proposed that the interaction between two electrically charged spheres can be expressed as:

$$\boldsymbol{f} = -\frac{edl}{\kappa}\, e^{-\kappa d_p} + \frac{A\, r_p}{6\, d_p^2} \tag{8}$$

where the first term on the right hand side is due to the electric double layer, and the second is due to van der Waals potential, with $edl \equiv 64\,\pi r_p n\, k_B T_F \gamma^2$ for the electric double layer. A is the Hamaker constant, n is the number density of electrolyte ions, $\gamma = \tanh\left(\frac{z\, e\, \psi}{4\, k_B T_F}\right)$, ψ is the reduced surface potential, κ is the inverse Debye length, T_F is the fluid temperature, d_p is the inter-surface distance and k_B is the Boltzmann constant.

The parameters associated with calcite particles in water are presented in Table 2.

Table 2: Parameters for calcite particles.

Parameter	r_p	e	ρ_p/ρ_F	A	n	θ	κ	T_F
Value	$50\mu m$	0.4	2.71	$22.3\ zJ$	$10^{-3}M$	$20mV$	$0.1/nm$	$300K$

3 RESULTS AND DISCUSSION

Validation of the IBM used in the simulations was performed in [10], reported here for completeness. It was based on comparing the simulated drag force on an icosphere with 20, 80 and 320 faces against empirical values [13]. The results of those simulations are presented

in Fig. 2. The results show that as the number of faces on the icosphere is increased, the simulated drag force increases in accuracy until at 320 faces the predicted and empirical values are in close accord. In the present work, 320 faces represented a good compromise between accuracy and computational cost.

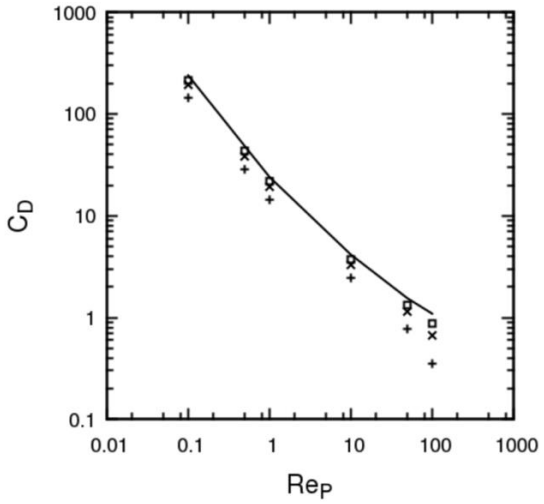

Figure 2: Simulated drag coefficient for icosphere face subdivisions, N_f, of 20 (+), 80 (×) and 320 (□) compared against empirical values (—).

The results presented in Fig. 3 for the isotropic boxes at $Re_\lambda = 29$ and $Re_\lambda = 197$ were validated against the predictions of Rosales and Meneveau [9]. The figure shows the time evolution of the total rms of the fluid velocity fluctuation field. The predictions show that the rms values ultimately reach statistically stationary values of 0.244 and 0.581 for boxes representative of the bulk flow and viscous sub-layer regions, respectively, with these values being in good agreement with those of Rosales and Meneveau [9].

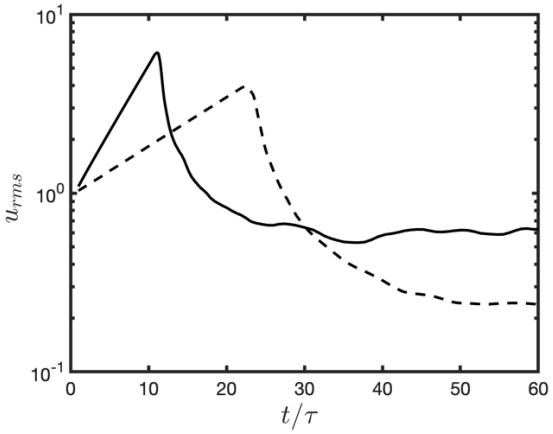

Figure 3: Time evolution of rms of fluid velocity fluctuations in the isotropic boxes (— $Re_\lambda = 197$ and --- $Re_\lambda = 29$).

Figure 4 shows the variation of Re_λ across a steady $Re_\tau = 180$ turbulent channel flow in

the wall normal direction. As we move from the bulk flow region ($y^+ = 36$ to 180) to the viscous sub-layer region ($y^+ = 0$ to $y^+ = 5$) Re_λ increases exponentially as the viscous region is approached, and then drops to zero at the wall. If Re_λ is used as a measure of turbulence, then the various regions in a turbulent channel flow can be simulated as an isotropic turbulent box by generating the required level of Re_λ in the box. By studying the particle dynamics using IBM in such isotropic boxes, the characteristic features of particle interactions, collisions and agglomeration in particular regions of the turbulent channel flow can be examined in detail.

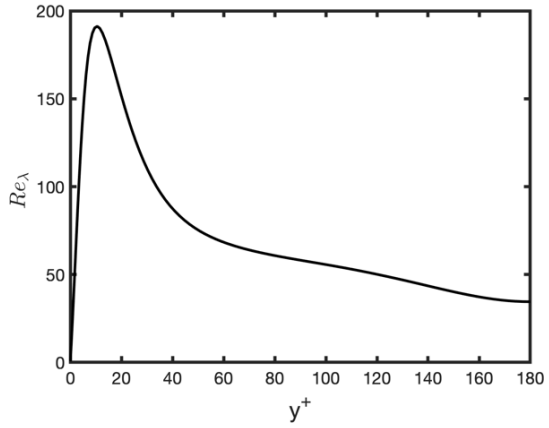

Figure 4: Variation of Re_λ in the wall normal direction of a $Re_\tau = 180$ turbulent channel flow.

Figures 5 and 6 show PDFs of the particle collision velocity and collision angles obtained from LPT simulations of a $Re_\tau = 180$ turbulent channel flow at $St_k = 1$ for the bulk flow and viscous sub-layer regions [14]. The most probable velocities and angles from these results were used as initial conditions for the isotropic box simulations to investigate the interaction of particles in those regions. In the two regions, the most probable collision velocity is dominated by the streamwise direction, with the corresponding collision angles indicating that collisions in the bulk flow region are generally at very low angles, almost head-on, whilst those in the viscous sub-layer show a wider distribution of angles.

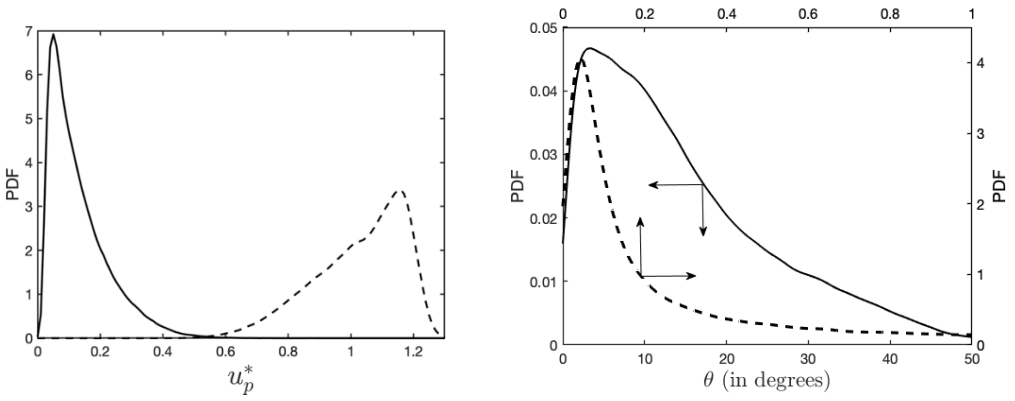

Figure 5: PDFs of streamwise particle collision velocity (left) and collision angle (right), both in viscous sub-layer and bulk flow regions of $Re_\tau = 180$ turbulent channel flow (— $Re_\lambda = 197$ and --- $Re_\lambda = 29$).

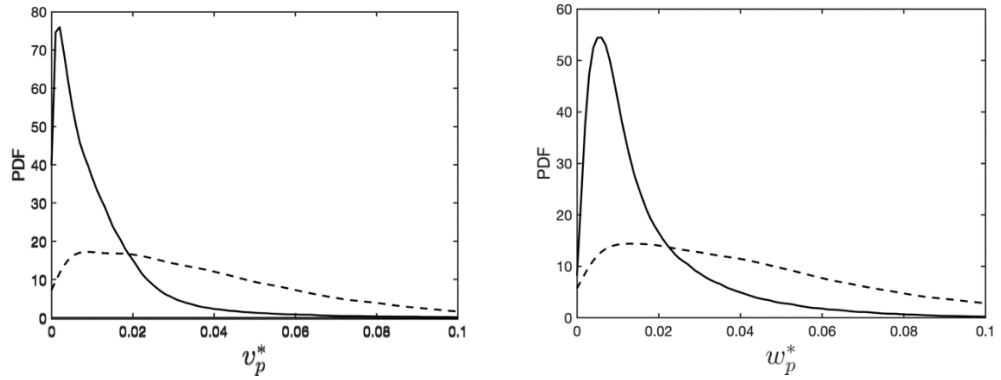

Figure 6: PDFs of wall-normal (left) and spanwise (right) particle collision velocities, both in viscous sub-layer and bulk flow regions of $Re_\tau = 180$ turbulent channel flow (— $Re_\lambda = 197$ and --- $Re_\lambda = 29$).

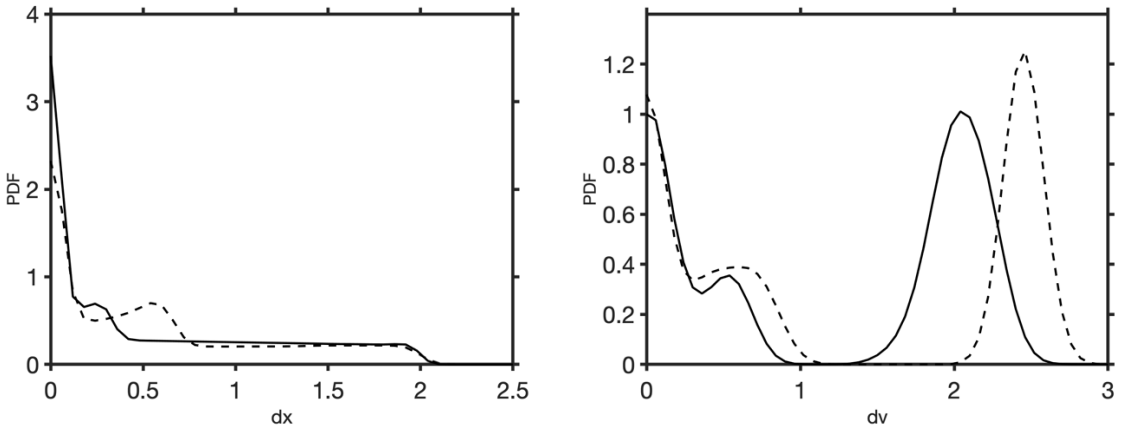

Figure 7: PDFs of particle displacement (left) and particle relative velocity (right) in the two isotropic turbulence boxes (— $Re_\lambda = 197$ and --- $Re_\lambda = 29$).

Figure 7 shows PDFs of the magnitude of particle displacement and particle relative velocity in each isotropic box, at $Re_\lambda = 197$ (representative of the viscous sub-layer) and $Re_\lambda = 29$ (representative of the bulk flow). The PDFs were obtained by recording the displacement and the relative velocity after each time-step of the simulations, until the 2000th time-step had been reached. After this time, the whole process was restarted by randomly distributing the particles in the box whilst keeping their initial inter-surfacial displacement fixed at $2d_p$.

To analyse the distributions given in Fig. 7, first we consider the displacement of the particles. In the figure, $dx = 2$ represents the initial displacement and $dx = 0$ represents contact of the particles and their possible agglomeration. The two PDFs are similar in terms of their profile in that a peak at $dx = 0$ is observed, indicating interactions which resulted in agglomeration. The larger peak for the viscous sub-layer region suggests that interactions at $Re_\lambda = 197$ resulted in the particles spending more time in an agglomerated state. In both

cases, the PDF drops exponentially as the inter-surfacial distance is increased from $dx = 0$. At $dx \sim 0.25$ (viscous sub-layer) and $dx \sim 0.5$ (bulk flow) each PDF exhibits a minor secondary peak, which is the result of bounces to these separation distances. It is clear that the particles in the bulk flow region bounce almost twice as far as those in the viscous sub-layer. Over the range $0.8 \leq dx \leq 2.0$ the results are almost identical in both case since this is the range over which the particles initially travel as they approach one another. This indicates that during this time turbulence does not significantly affect the relative distance between the particles, which in turn means that all the effects due to turbulence over this period are on the translational and angular motion of the particles. Overall, the results given in this figure demonstrate that the particles in the viscous sub-layer box lose more kinetic energy due to collisions than those in the bulk flow box, which can be attributed to the hydrodynamic forces acting on the particles caused by the turbulence. This indicates that particles in the viscous region at this Stokes number are more likely to agglomerate than particles in the bulk flow region as they lose more energy after any collision which increases the impact of local hydrodynamic forces.

Considering the relative velocity PDFs, in Fig. 7 $dv = 2.5$ represents the initial relative velocity of the particles and $dv = 0$ indicates that the particles have agglomerated (such that they travel with the same velocity). Despite initiating the particles with the same initial relative velocity of 2.5 in both the viscous sub-layer and bulk flow boxes, the particles in the former case lose a significant amount of their velocity, ~20%, equivalent to a loss ~36% of their kinetic energy, in the first few time-steps due to turbulence interactions. As when considering particle displacement, over the range $0.0 \leq dv \leq 1.1$ collisions, bouncing and agglomeration of the two particles occur. The difference due to their initial approach velocity can be seen in the range $0.2 \leq dv \leq 1.1$. In that range, as the particles bounce off one another, the particles in the bulk flow box tend to move faster than those in the viscous sub-layer box, thereby reducing the chance of agglomeration due to their retained speed.

From the analysis of the distribution of both the relative displacement and velocity of the interacting particles, it is therefore clear that agglomeration of particles can occur in both the viscous sub-layer ($Re_\lambda = 197$) and bulk flow ($Re_\lambda = 29$) boxes. However, agglomeration is much more likely in the viscous sub-layer due to significant reductions in the particles' kinetic energy post-collision, in this case a reduction of ~36%.

4 CONCLUSIONS

Direct numerical simulations of boxes of isotropic turbulence were performed using the Nek5000 code based on a 7th-order spectral element method, from which good agreement with the results from Rosales and Meneveau [9] was established. An immersed boundary method using icospheres and inelastic hard sphere collisions was used to describe inter-particle interactions, with inter-particle forces modelled using DLVO theory. Validation of the IBM was performed by comparing the calculated drag force on icosphere particles with 20, 80 and 320 triangular faces with empirical values, with good agreement found for the more resolved icosphere case.

Two regions of a turbulent channel flow were represented using these isotropic boxes at differing values of Re_λ, representative of those occurring in the viscous sub-layer and bulk flow regions of the channel. PDFs of inter-particle interactions, in this case the particle

relative displacement and velocity, were analysed. In both the bulk flow and viscous sub-layer cases, agglomeration was found to occur, but the chances of agglomeration were increased in the viscous sub-layer box. The results indicate that particles in the viscous box lose significantly more kinetic energy after particle impact than in the bulk flow case. Furthermore, in the first few time-steps of a simulation, particles in viscous sub-layer box lost ~20% of their initial velocity, which translates into a loss of ~36% of their kinetic energy which in turn encourages agglomeration of the particles.

Ultimately, this work aims to use simulations of the type described to assess the use of adjustable system parameters to encourage or discourage particle agglomeration in turbulent flows. Through such behavioural modification, it may be possible to accelerate nuclear waste removal and treatment processes in addition to reducing their cost. Future work will also extend these simulations and analysis to cover more realistic non-spherical particles such as prolate and oblate ellipsoids, representative of the needle- and disc-like particles encountered in practice.

5 ACKNOWLEDGEMENTS

This work was supported by a UK Engineering and Physical Sciences Research Council (EPSRC) grant to the University of Leeds from the EPSRC Centre for Doctoral Training in Nuclear Fission – Next Generation Nuclear.

REFERENCES

[1] Maxey, M.R. and Riley, J.J. Equation of motion for a small rigid sphere in a nonuniform flow. *Phys. Fluids* (1983) **26**: 883-889.

[2] Peskin, C.S. Flow patterns around heart valves: A numerical method. *J. Comput. Phys.* (1972) **10**:252-271.

[3] Mark, A. and van Wachem, B.G.M. Derivation and validation of a novel implicit second-order accurate immersed boundary method. *J. Comput. Phys.* (2008) **227**:6660-6680.

[4] Tseng, Y.H. and Ferziger, J.H. A ghost-cell immersed boundary method for flow in complex geometry. *J. Comput. Phys.* (2003) **192**:593-623.

[5] Elghobashi, S. On predicting particle-laden turbulent flows. *Appl. Sci. Res.* (1994) **52**:309-329.

[6] Elghobashi, S. An updated classification map of particle-laden turbulent flows. *Proc. IUTAM Symp. Computational Approaches to Multiphase Flow* (2004) 3-10.

[7] Fischer, P.F., Lottes, J.W. and Kerkemeier, S.G. Nek5000 Web page, http://nek5000.mcs.anl.gov (2008).

[8] Lundgren, T.S. Linearly forced isotropic turbulence. *Annual Research Briefs*, Center for Turbulence Research (2003) 461-473.

[9] Rosales, C. and Meneveau, C. Linear forcing in numerical simulations of isotropic turbulence: Physical space implementations and convergence properties. *Phys. Fluids* (2005) **17**:095106.

[10] Mortimer, L.M., Fairweather, M., and Njobuenwu, D.O. Simulation of fully resolved particle-particle interaction in turbulence with behavioural modification. *10th International Conference on Multiphase Flow* (2019) Paper OC.389.

[11] Derjaguin, B. and Landau, L. Theory of the stability of strongly charged lyophobic sols and of the adhesion of strongly charged particles in solutions of electrolytes. *Acta Physicochim.* (1941) **14**:633-662.
[12] Verwey, E.J.W. and Overbeek, J.T.G. Theory of the stability of lyophobic colloids. *J. Colloid Sci.* (1955) **10**:224-225.
[13] Rouson, D.W. and Eaton, J.K. On the preferential concentration of solid particles in turbulent channel flow. *J. Fluid Mech.* (2001) **428**:49-169.
[14] Rai, K., Mortimer, L.F. and Fairweather, M., Effect of Reynolds number on critical Stokes number in turbulent channel flow. *10th International Conference on Multiphase Flow* (2019) Paper OC.056.